Supplementary Information for

Title: Thermodynamic phase transitions reveal the resilience structure of urban traffic congestion

Contents

Supplementary Notes

Supplementary Note 1: Data Source

Urban traffic conditions were characterized using a combination of floating-car data and fixed traffic detector measurements. The analysis relies exclusively on provider-processed

and publicly released aggregate indicators; no raw data reconstruction or individual-level processing was performed. Because the spatial units used in the COVID-period mobility datasets do not necessarily coincide exactly with the metropolitan polygons defined in the congestion datasets, perfect spatial alignment cannot be verified. However, since the mobility indicators are expressed as relative percentage changes rather than extensive quantities, moderate variations in polygon boundaries are not expected to materially affect the congestion–mobility relationships analyzed here.

Traffic Congestion Index (TCI)

Traffic congestion is measured using the Traffic Congestion Intensity (TCI) as defined in the Inter-American Development Bank (IDB) Coronavirus Impact Dashboard framework (1). The IDB accesses aggregate Waze data through the Waze for Cities Program.

Waze identifies traffic jams as contiguous road segments ("jam lines") where observed speeds fall below expected free-flow conditions. Jam lines are reported at 5-minute intervals. For each metropolitan area (polygon p), total jam length at interval i is defined as

$$JAM_{ip} = \sum_j L_{jip}, \qquad (1)$$

where L_{jip} is the length of jam line j within polygon p.

Daily Traffic Congestion Intensity is computed as:

$$TCI_{pt} = \sum_{i \in t} JAM_{ip} \quad (2)$$

where t denotes a full day. By construction, TCI_{pt} captures both the spatial extent and temporal persistence of congestion (see Supplementary Fig. S1 for a schematic illustration).

To evaluate changes over time, the IDB defines March 2–8, 2020 as the baseline week and applies day-of-the-week matching. The percentage change in congestion is defined as

$$\Delta TCI_{pdt1} = \left(\frac{TCI_{pdt1}}{TCI_{pdt0}} - 1\right) \times 100. \quad (3)$$

This study relies exclusively on aggregate ΔTCI_{pdt1} indicators as reported by the IDB. For simplicity, in the main text we denote this quantity as TCI. No raw jam geometries or user-level data are accessed.

The dataset metadata include the polygon boundaries, total road network length, metropolitan population, TCI_{pdt1}, and TCI_{pdt0}. Selected descriptive properties of these variables are shown in Supplementary Fig. S1.

TomTom Traffic Index and Vehicle Miles Traveled (VMT)

The TomTom Traffic Index (2) is constructed from proprietary floating-car data collected through navigation devices, connected vehicles, and mobile applications at the city scale. The index measures the additional travel time experienced by drivers relative to free-flow conditions due to congestion and is reported as a percentage increase over free-flow travel time.

Waze also provides a city-level measure of Vehicle Miles Traveled (VMT), representing total driving activity aggregated across users. VMT is expressed as relative changes with respect to predefined baseline periods.

Both indicators are expressed relative to free-flow conditions and are used in this study solely as external benchmarks for comparative analysis. They are not used to compute the main congestion metric introduced here (see Fig. 2B–C in the main text and Supplementary Figs. S5–S6).

Historical city-level time series for both metrics were obtained from archived mobility repositories compiled during the COVID-19 period (3).

In addition, the TomTom Traffic Index value shown in Fig. 2E corresponds to the official 2023 city congestion ranking (2), as published on the TomTom Traffic Index website. This value is used as a cross-sectional reference and is not part of the time-series analysis.

Google COVID-19 Community Mobility Reports

Mobility data were obtained from the Google COVID-19 Community Mobility Reports(4)**,** which provide daily percentage changes in visits to different place categories relative to a pre-pandemic baseline. The data are generated from aggregated, anonymized location information from users who have opted into Google Location History.

Here, only the *Workplaces* category is used. This indicator reflects daily relative changes in work-related activity and commuting demand and is treated as the mobility variable. The *Workplaces* time series were restricted to the common observation window (March 9, 2020 to May 5, 2022) and aligned with congestion indicators at daily resolution. When required for comparative analysis, mobility was linearly rescaled to a dimensionless form without altering its temporal structure.

Throughout the analysis, the Workplaces indicator is interpreted as a control parameter (M in main text) governing the macroscopic state of the urban traffic system, while congestion metrics quantify the system's aggregate response.

Urban traffic detector dataset (UTD19)

Fixed traffic detector data were obtained from the UTD19 dataset (5)**,** a large-scale urban traffic dataset compiled by the Institute for Transport Planning and Systems (IVT) at ETH

Zurich**.** UTD19 consists of measurements from stationary detectors (loop detectors) deployed on urban roads in more than 40 cities worldwide. The dataset includes traffic variables such as vehicle flow, occupancy, and speed, reported at short aggregation intervals (typically 3–5 minutes; 1 hour for Paris). It also provides link-level metadata, including segment length, number of lanes, and road functional classification. The dataset spans multiple years and comprises billions of detector observations.

These data have been widely used to study empirical properties of urban traffic, including the macroscopic fundamental diagram (6–9). In this study, no additional processing was applied beyond temporal aggregation consistent with other data sources and the conversion of occupancy measurements into density estimates. From the full set of cities, we retained those with sufficiently dense detector coverage across the urban area. This filtering resulted in eight cities: Bordeaux, London, Los Angeles, Madrid, Paris, Rotterdam, Taipei, and Torino.

Supplementary Note 2: **Definition of macroscopic variables**

Here we define the macroscopic observables used to characterize the collective state of urban traffic systems.

Density ρ

Road segment density ρ(veh/km) is estimated from loop-detector occupancy measurements. Occupancy O, is defined as the fraction of time during which a given lane detector is occupied within an aggregation interval. For each detector lane, density is computed as

$$\rho = \frac{O}{Ldet+Lv}\ x1000 \quad (4)$$

where:

- O is occupancy in fractional form,
- $Ldet$ is the effective detector segment length (m),
- Lv is the assumed average vehicle length (m),
- the factor 1000 converts units from veh/m to veh/km.

Because loop detectors operate at the lane level, density is defined in units of veh/km/lane. Network-level density is obtained by aggregating lane-level densities using the median across all available detector lanes at each time interval. The median is used instead of the mean because the empirical distribution of densities exhibits a heavy-tailed (approximately power-law) behavior. Thus, the mean can be disproportionately influenced by extreme values, whereas the median provides a more robust estimate of the typical macroscopic load of the network.

Volume-over-Capacity (VOC)

Volume-over-capacity is defined as $VOC = \frac{q}{C}$, where q is observed flow and C is the assumed lane-level capacity of the corresponding road segment.

Capacity values are assigned according to the OpenStreetMap functional road classification of each link. A fixed capacity map is used:

- motorway: 2200 veh/h/lane
- trunk: 2400
- primary: 2200
- secondary: 1900
- tertiary: 1400
- living_street: 400
- unclassified: 700

motorway_link: 2000
trunk_link: 2000
primary_link: 1800
secondary_link: 1500
residential: 900
service: 600
other: 1000

Capacities are expressed in vehicles per hour per lane and are treated as nominal operating limits representative of typical urban conditions. Network-level VOC is computed as the mean across detector lanes at each time interval. The main results are robust to moderate variations in the assumed capacity values, as such variations produce only small rescalings of VOC without altering the observed macroscopic relationships.

Jam Fraction p_{jam}

The jam fraction p_{jam} is defined as the fraction of monitored links classified as congested at a given time interval, $p_{jam} = \frac{N_{jam}}{N_{total}}$, where N_{jam} is the number of detector lanes exceeding a congestion threshold and N_{total} is the total number of monitored lanes. A lane is classified as congested when its density exceeds a road-type–specific threshold, $\rho > \rho_{th}$.

The density thresholds ρ_{th} (veh/km/lane) are assigned according to functional road classification, consistent with critical density ranges reported in the traffic flow literature for freeways, urban arterials, and local streets:

- motorway, motorway_link, trunk, trunk_link: 45 veh/km/lane
- primary: 45
- primary_link: 35
- secondary: 33
- secondary_link: 30
- tertiary, residential, living_street, service, unclassified, other: 30

These values fall within empirically observed ranges of critical density associated with the onset of congestion across road classes. Results are insensitive to reasonable variations in the assumed density thresholds values.

Supplementary Note 3: Statistical Estimation Procedures

This section describes the procedures used to estimate the macroscopic transition and associated parameters.

Binning Protocol

All macroscopic relationships were estimated using fixed-width binning in the corresponding control variable (e.g., density ρ or mobility M). For each city, observations were grouped into equal-width bins, and the mean value of the associated macroscopic observable (e.g., jam fraction p_{jam} percentage change in TCI, or reconstructed free-energy derivatives) was computed within each bin. Bins with insufficient observations were excluded. This coarse-graining procedure was applied consistently across all sigmoidal and free-energy analyses.

Estimation of the Sigmoidal Transition

Sigmoidal transitions were estimated by nonlinear least-squares fits using `curve_fit`.

For the jam fraction–density relationship, we used a hyperbolic tangent form:

$$p_{jam}(\rho) = \frac{p_{max}}{2}\left[1 + tanh\left(\frac{\rho - \rho_c^{(emp)}}{\Delta}\right)\right], \quad (5)$$

where $\rho_c^{(emp)}$ is the transition midpoint and Δ controls the transition width.

An analogous procedure was applied to the congestion–mobility relationship using the Traffic Congestion Intensity (TCI). The empirical TCI–mobility curve was fitted with the same functional form, with L corresponding to the saturation value TCImax.

To enable comparison with the canonical two-state formulation, the fitted TCI was normalized as $\langle m \rangle = \frac{TCI}{TCI_{max}}$, and transformed into a centered order parameter, $2\langle m \rangle - 1$.

Fits were performed using `curve_fit` with weighted least squares, providing bin-level uncertainties σ (std error) as weights (via the `sigma` argument). Goodness-of-fit (R^2) values were computed using the binned median data used for parameter estimation.

Supplementary Note 4: Free-energy derivation of the sigmoidal jam transition

Effective free-energy formulation

We describe the macroscopic congestion state of the monitored road network through the fraction of jammed links ppp, treated as a collective order parameter. The mean network density ρ acts as the externally controlled variable.

We introduce an effective free energy $F(\Delta,\rho) \sim \kappa_{city}\left(\langle VOC\rangle - \frac{\Delta}{\rho_{th}}S\right)$ (Eq. 5 in the main text), where $S(p) = -p_{jam}\, ln\, p_{jam} - (1-p_{jam})ln(1-p_{jam})$ is the binary entropy associated with jammed and free links. Here Δ represents an effective temperature (expressed in density units) controlling the width of the transition, and ρ_{th} is the characteristic jam-density threshold defining the binary congestion state of a road segment.

In the main text we define the transition width parameter $\Delta \equiv T_{jam}\rho_c^{(emp)}$.

Energetic term and throughput interpretation

The energetic contribution is taken proportional to the average $\langle E\rangle = \langle VOC\rangle = \langle\frac{q}{C}\rangle$, where q denotes traffic flow and C the link capacity.

Using the macroscopic traffic identity $\langle q\rangle = \rho\, v(\rho, p_{jam})$, and approximating $\langle\frac{q}{C}\rangle \approx \frac{\langle q\rangle}{\langle C\rangle}$, we obtain

$$\langle E\rangle(\rho, p_{jam}) \propto \frac{\rho\, v(\rho,p_{jam})}{\langle C\rangle}. \quad (6)$$

Consistent with classical two-fluid descriptions of traffic, we empirically observe an approximately linear relation between average velocity and the fraction of jammed links (Supplementary Fig. S8),

$$v(\rho, p_{jam}) = v_{max}[1 - \gamma p_{jam}] \quad (7)$$

where γ quantifies the sensitivity of average velocity to the fraction of jammed links. This equation resembles the two-fluid formulation of urban traffic proposed by Prigogine and Herman(10), where the macroscopic speed of the system is determined by the fraction of vehicles that belong to the congested phase.

At the link level, the maximum observed flow $q_{\ max}$ is the observed corresponds to the operational capacity of the link. Under a triangular fundamental-diagram approximation, the characteristic maximum flow satisfies

$$\langle q_{\ max}\rangle \approx \rho_{th}\, v_{max} \quad (8)$$

Because designed link capacities are prescribed by road class, this scale is proportional to the nominal capacity, so that

$$\rho_{th}\, v_{max} \approx \eta\langle C\rangle \quad (9)$$

where η= O(1) is a dimensionless proportionality factor that absorbs deviations from an ideal triangular diagram and the mapping between the threshold density imposed in our classification and the density at capacity.

Substituting this relation yields

$$\langle E\rangle(\rho, p_{jam}) = \frac{\rho}{\eta\,\rho_{th}}(1 - \gamma p_{jam}). \quad (10)$$

Hence

$$\left.\frac{\partial\langle E\rangle}{\partial p_{jam}}\right|_{\rho} = -\frac{\gamma}{\eta}\frac{\rho}{\rho_{th}}. \quad (11)$$

Minimization and logistic form

Equilibrium at fixed density ρ is obtained from

$$\left.\frac{\partial F}{\partial p_{jam}}\right|_{\rho} = 0, \quad (12)$$

which gives

$$\left.\frac{\partial\langle E\rangle}{\partial p_{jam}}\right|_{\rho} - \frac{\Delta}{\rho_{th}}\frac{\partial S}{\partial p_{jam}} = 0. \quad (13)$$

Since

$$\frac{\partial S}{\partial p_{jam}} = -\ln\frac{p_{jam}}{1-p_{jam}}, \quad (14)$$

we obtain

$$\ln\frac{p_{jam}}{1-p_{jam}} = -\frac{\rho_{th}}{\Delta}\left.\frac{\partial\langle E\rangle}{\partial p_{jam}}\right|_{\rho}. \quad (15)$$

Substituting the energetic derivative leads to $\ln\frac{p_{jam}}{1-p_{jam}} = -\frac{\gamma}{\eta\Delta}\rho$. Introducing the transition density ρ_c such that p_{jam}=1/2 when $\rho = \rho_c$, the equilibrium condition can be written in centered form

$$\ln\frac{p_{jam}}{1-p_{jam}} = -\frac{\gamma}{\eta\Delta}(\rho - \rho_c). \quad (16)$$

This form ensures that the order parameter varies linearly with the control parameter in the vicinity of the transition, consistent with the empirically observed sigmoidal transition.

Therefore,

$$p_{jam}(\rho) = \frac{p_{max}}{1+exp\left[-\frac{\gamma(\rho-\rho_c)}{\eta\Delta}\right]}, \quad (17)$$

where p_{max} represents the empirical saturation level of the jam fraction.

Equivalently, defining the symmetric order parameter $\langle m \rangle = 2p_{jam} - 1$, or

$$p_{jam}(\rho) = \frac{p_{max}}{2}\left[1 + \tanh\left(\frac{\gamma(\rho - \rho_c)}{2\eta\Delta}\right)\right] \qquad (18)$$

Up to multiplicative constants absorbed in the definition of the transition width, this expression corresponds to the sigmoidal form used in the main text.

This derivation shows that the sigmoidal transition of the jam fraction emerges naturally from three minimal ingredients:

- a coarse-grained binary description of congestion states,
- an energetic term proportional to normalized network density, and
- a linear dependence of average velocity on the jam fraction.

No assumptions are made about the detailed microscopic distributions of density or velocity; these enter only through renormalized parameters ρ_c and Δ.

The resulting logistic equation therefore represents the equilibrium relation between network density and the macroscopic congestion state.

Supplementary Note 5: Reconstruction of Free Energy

Although congestion at the link level is characterized by a continuous variable (volume-over-capacity, VOC), empirical observations reveal two dominant macroscopic regimes corresponding to uncongested and congested network states. Motivated by this bimodal structure, we reconstruct an effective free-energy profile as a function of the network density ρ\rhoρ using the canonical two-state functional form

$$F(\Delta, \rho) = F_0 - \frac{p_{max}}{2}\Delta \ln\left[2cosh\left(\frac{\rho - \rho_c^{(fit)}}{\Delta}\right)\right]. \qquad (19)$$

Here F_0 is an additive constant, $\rho_c^{(fit)}$ is the transition density obtained from the sigmoidal fits, and Δ is the empirically determined transition width, corresponding to the effective temperature expressed in density units.

Taking the derivative with respect to ρ yields

$$\frac{\partial F}{\partial \rho} \propto tanh\left(\frac{\rho - \rho c}{\Delta}\right), \quad (20)$$

which reproduces the sigmoidal dependence of the macroscopic order parameter observed in the data.

The constant F_0 does not affect the transition properties and only shifts the potential vertically. Fits were performed using weighted nonlinear least squares together with the binning protocol described above.

Mobility as Control Parameter (City-Level Analysis)

At the city scale (Figs. 1–2 in the main text), mobility M is used as the control variable instead of density. Because increased mobility loads the road network, average density is empirically observed to vary monotonically with mobility over the analyzed period. Mobility therefore acts as a natural proxy control parameter for the macroscopic transition.

In this representation, the transition width Δ plays the role of an effective temperature, we called it T, governing the smoothness of the congestion transition. When mobility is expressed in normalized (dimensionless) units, Δ is also dimensionless.

By contrast, in the density-based reconstruction, the transition width retains the units of density (veh/km/lane) and therefore represents a temperature-like parameter defined on the density scale rather than a normalized variable.

After normalizing TCI by its empirical saturation value TCI_{max}, $\langle m \rangle = \frac{TCI}{TCI_{max}}$, and centered as $2\langle m \rangle - 1$, making it directly comparable to the canonical two-state expectation.

In this normalized mobility representation, no additional scale factor (κ_{city}) is required, and the effective temperature is fully determined by the sigmoidal transition width.

Parameter Roles and Identification

For clarity, we summarize the estimation status of all parameters introduced in the sigmoidal and free-energy reconstructions:

- ρ_c: empirically estimated from sigmoidal fits.
- Δ: estimated from the sigmoidal transition and fixed in the free-energy reconstruction.
- κ_{city} : scale factor estimated in free-energy fits (absorbing normalization and sampling effects).
- F0: additive offset without thermodynamic interpretation.

No additional free parameters are introduced beyond those explicitly stated.

Although urban traffic exhibits microscopic interactions (e.g., spillbacks and queue propagation), the present formulation is macroscopic and effective. The free-energy form summarizes the collective outcome of such interactions without modeling explicit pairwise couplings. In this sense, the canonical expression is phenomenological rather than mechanistic.

Interpretation and limitations

This noninteracting formulation provides a minimal explanation for the observed sigmoidal mobility–congestion relationship and motivates a thermodynamic interpretation of urban

traffic states. Within this framework, mobility reshapes an effective free-energy landscape, and the observed congestion level corresponds to the equilibrium response of the system.

Deviations from this idealized behavior—such as hysteresis, metastability, or history-dependent effects observed in some cities—suggest the presence of interactions between road segments or temporal correlations not captured by the present formulation. The inclusion of explicit interaction terms (e.g., coupling between road segments) would modify the effective potential and could account for staircase-like or hysteretic behaviors observed in specific cases. These extensions remain a natural direction for future development of the framework.

Supplementary Figures

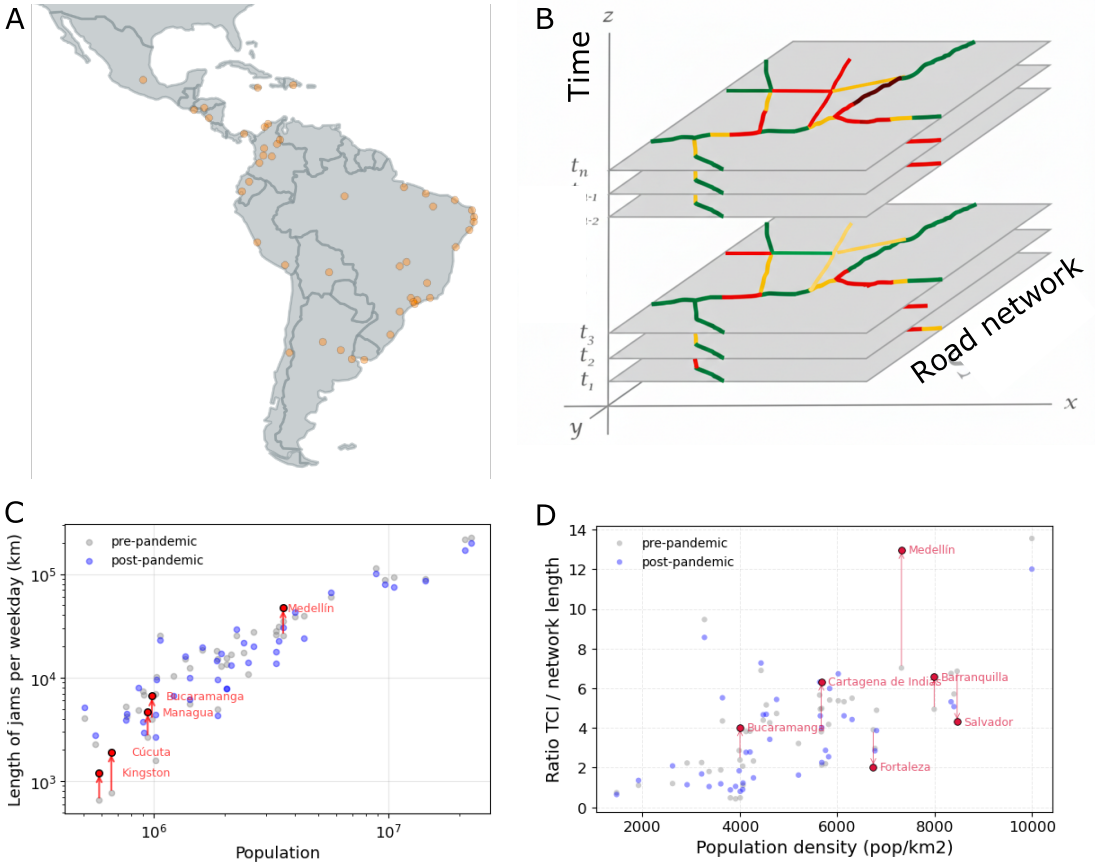

Supplementary Figure 1. Dataset coverage and construction of the Traffic Congestion Intensity (TCI). (A) Geographic distribution of metropolitan areas included in the IDB dataset for which Traffic Congestion Intensity (TCI) is computed. Dots indicate cities across Latin America and the Caribbean where sufficient Waze jam-line data are available. (B) Schematic illustration of TCI construction. Every 5 minutes, a network-wide snapshot is taken. Within each snapshot, all identified jam segments are extracted and their lengths summed. The daily TCI corresponds to the time-aggregated jam length across all 5-minute intervals, rescaled relative to the pre-pandemic baseline period. (C) Total daily jam length before and after the pandemic as a function of city population. In both periods, congestion scales with population approximately as a power law, P^{α}, consistent with urban scaling behavior. Cities exhibiting the largest post-pandemic deviations are highlighted. (D) Daily jam length normalized by network length as a function of population density. A roughly linear trend emerges, indicating that congestion intensity per unit infrastructure increases proportionally with density.

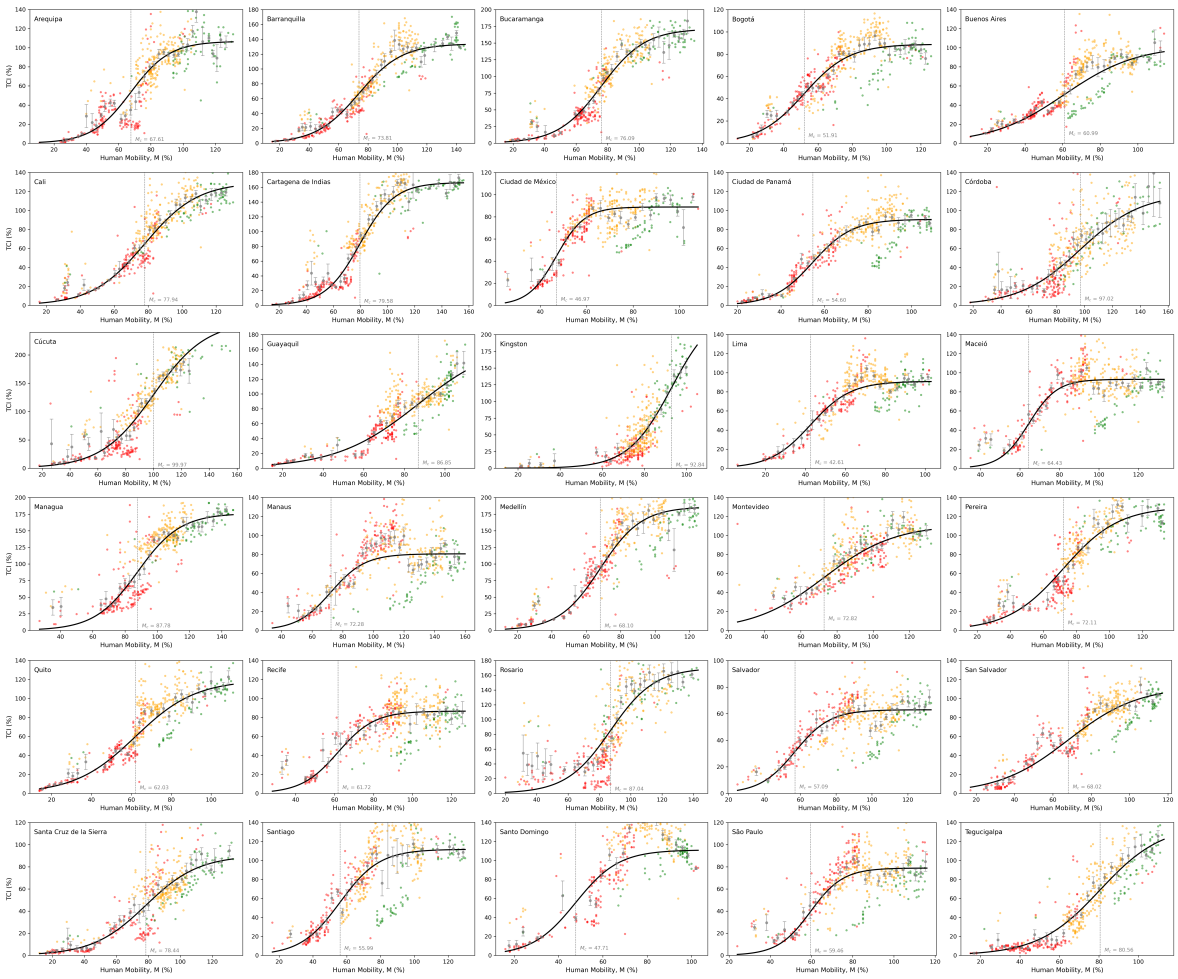

Supplementary Figure 2. Sigmoidal congestion transitions in daily Traffic Congestion Intensity across cities with high-quality fits. Each panel shows the daily Traffic Congestion Intensity (TCI) as a function of human mobility for cities with reliable sigmoidal reconstructions (31 cities, including Rio de Janeiro in the main text; all with fit quality R^2>0.8). Points are colored by year (2020 red, 2021 yellow, 2022 green). Solid black curves show the best-fit sigmoidal transition; error bars indicate binned variability. Because the underlying baselines for mobility and congestion differ across metropolitan areas (both in the x- and y-axes), direct cross-city comparison in raw units is not meaningful. This motivates the transformation used in the main text, where mobility is centered as $M - M_c$ and congestion is normalized into the magnetization-like variable $2\langle m \rangle - 1$, enabling collapse and comparison across cities. Several cities (e.g., Kingston, Guayaquil, and Tegucigalpa) do not exhibit a clear saturation plateau within the observed mobility range, suggesting that the system has not yet reached the high-congestion branch during the period analyzed. Notably, despite reported increases in private vehicle use in multiple cities (including Kingston, Medellín, Cartagena, Barranquilla, Cúcuta, Bucaramanga, and Rosario), Kingston still does not display saturation in TCI, consistent with a transition that remains incomplete over the available range. In such cases, T and M_c estimates are less constrained and should be interpreted cautiously.

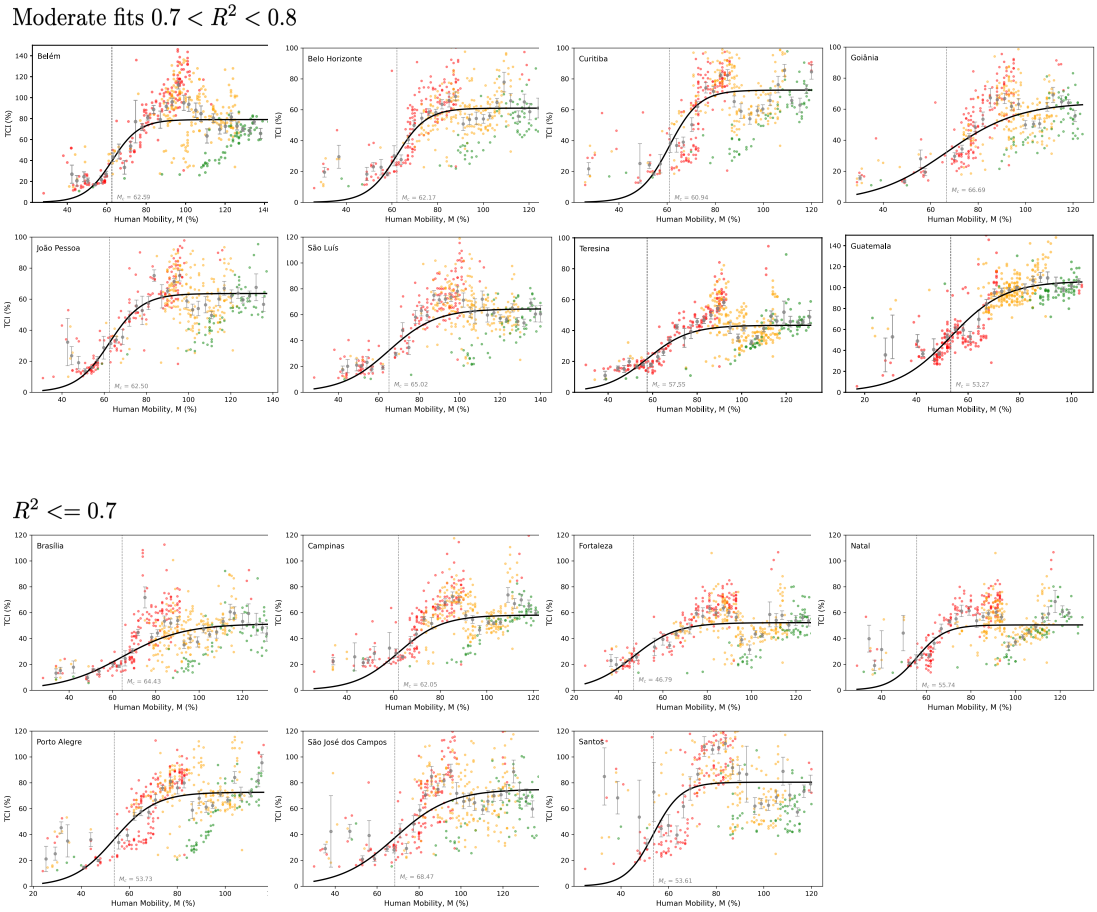

Supplementary Figure 3. Cities with intermediate and low-quality sigmoidal fits. Each panel shows daily Traffic Congestion Intensity (TCI) as a function of human mobility for cities where the sigmoidal reconstruction exhibits intermediate or low goodness of fit. Only 7 cities display poor fits, while the majority of cities continue to follow the transition structure described in the main text. Notably, 14 of the 15 lowest-quality fits correspond to Brazilian cities, many of them medium or small urban areas. During the pandemic period, Brazil experienced heterogeneous policy responses and mobility adherence patterns, these deviations coincide temporally with documented heterogeneity in mobility responses during the pandemic. In smaller metropolitan areas, such variability in mobility patterns may weaken the emergence of a well-defined sigmoidal transition, leading to noisier or structurally distorted congestion–mobility relations. Despite these deviations, the overall prevalence of robust sigmoidal fits across the dataset supports the generality of the transition framework.

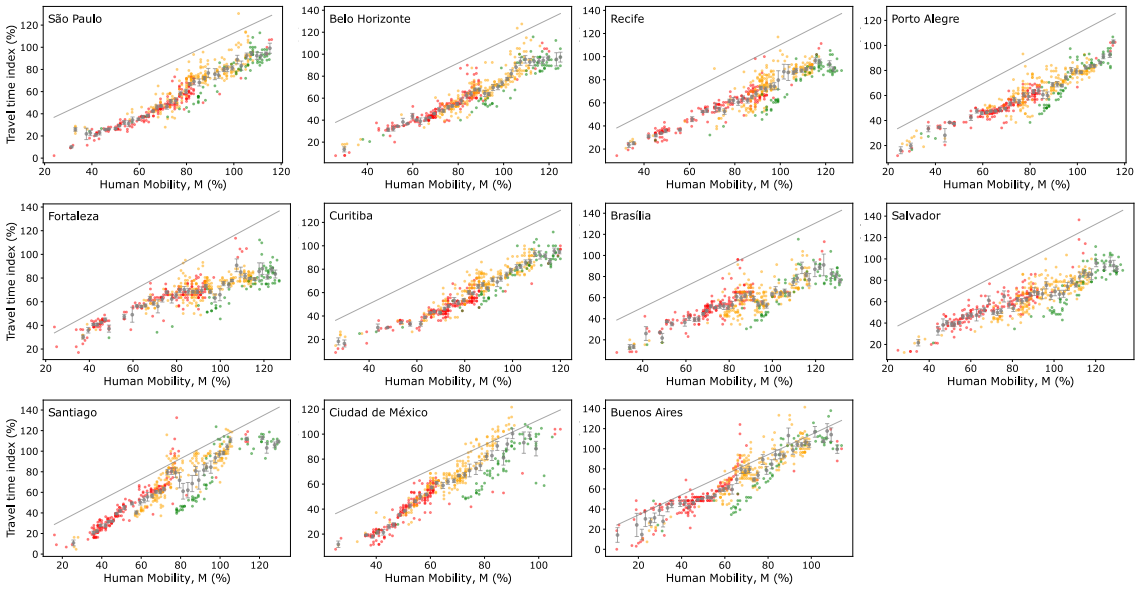

Supplementary Figure 4. Linear relationship between Travel Time Index and human mobility. Each panel shows the Travel Time Index (TTI, %) as a function of human mobility M (%) for the cities where TomTom data are available. Points are colored by year (2020 red, 2021 yellow, 2022 green). Across all cities, the relationship is approximately linear with slope close to unity, as indicated by the reference line. This proportionality suggests that, at the aggregate level, increases in mobility translate almost one-to-one into increases in travel time delays.

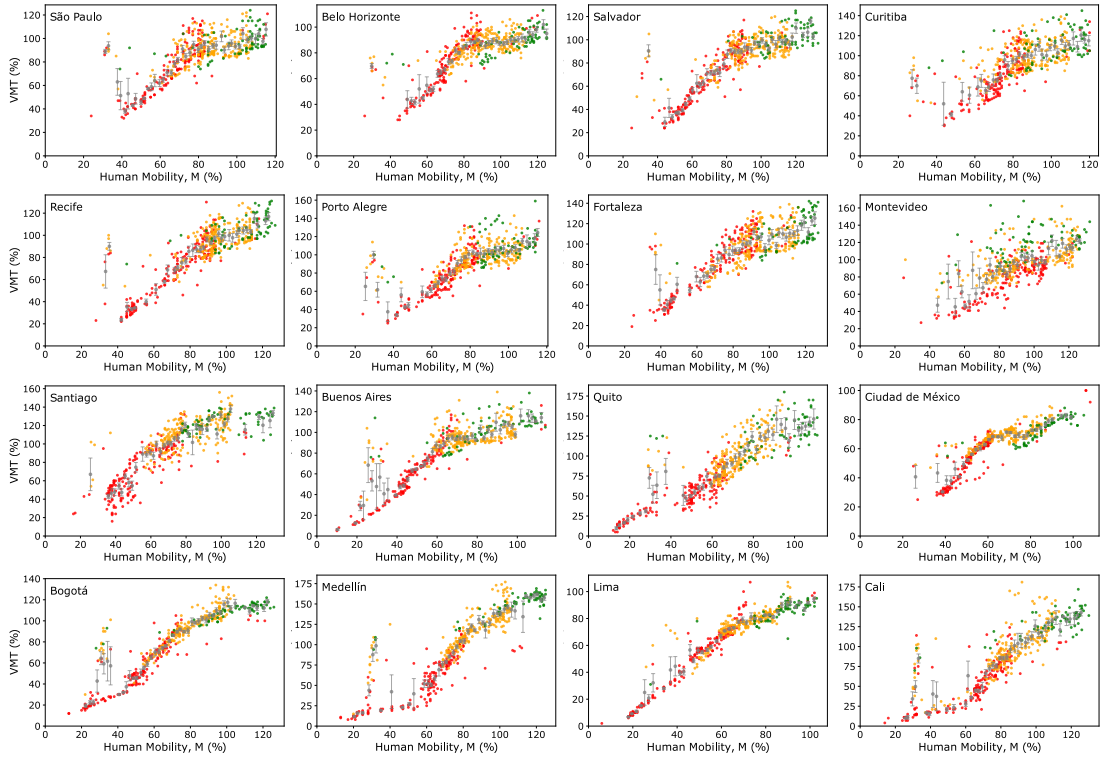

Supplementary Figure 5. Vehicle Miles Traveled (VMT) as a function of human mobility. Each panel shows total Vehicle Miles Traveled (VMT, %) versus human mobility M (%) for the cities where VMT data are available. Points are colored by year (2020 red, 2021 yellow, 2022 green). Across metropolitan areas,

VMT exhibits an approximately linear increase with mobility at low-to-intermediate values, followed by a progressive saturation at high mobility levels. This pattern mirrors the behavior reported in the main text, where macroscopic observables grow proportionally with mobility before approaching a capacity-limited regime. The saturation of VMT at high mobility suggests that increases in aggregate movement do not translate indefinitely into proportional increases in traveled distance, consistent with structural constraints imposed by network capacity.

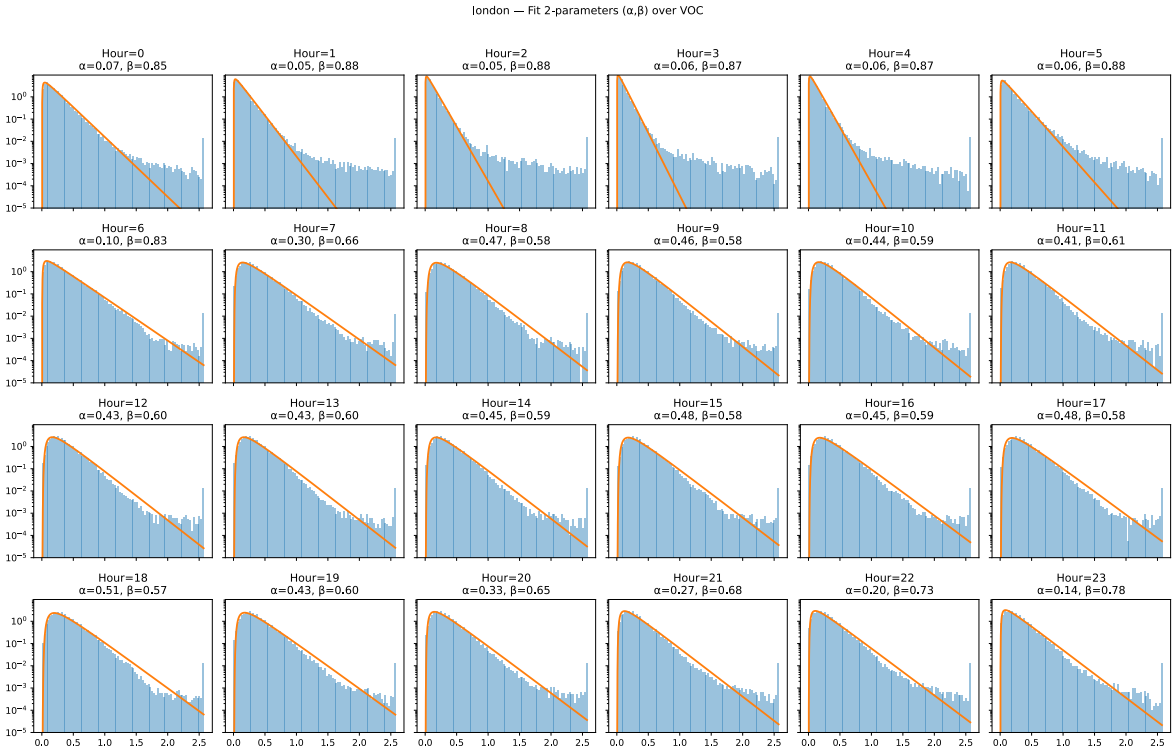

Supplementary Figure 6 (panel). Hourly fits of the normalized VOC distribution (London example). Histograms show the empirical distributions of normalized volume-over-capacity $x = \frac{VOC}{\langle VOC \rangle_t}$ for each hour of the day (0–23) in London. Solid curves correspond to two-parameter fits of the form $P_t(\mathrm{x}) \propto exp\,[-\alpha_t/x - \beta_t x]$. The fitted parameters α are indicated in each panel. While α varies systematically over the course of the day, reflecting changes in low-VOC behavior, the parameter β remains comparatively stable, particularly during daytime hours. The approximate constancy of β supports its interpretation as a temperature-like parameter governing the exponential decay of high-VOC states. The consistency of the functional form across all 24 hours indicates that the canonical-like structure of the VOC distribution is not restricted to specific time windows but persists throughout daily traffic cycles. The persistence of the functional form across all hours suggests that the canonical-like structure of the VOC distribution is a robust property of the system, rather than a transient artifact of specific traffic regimes.

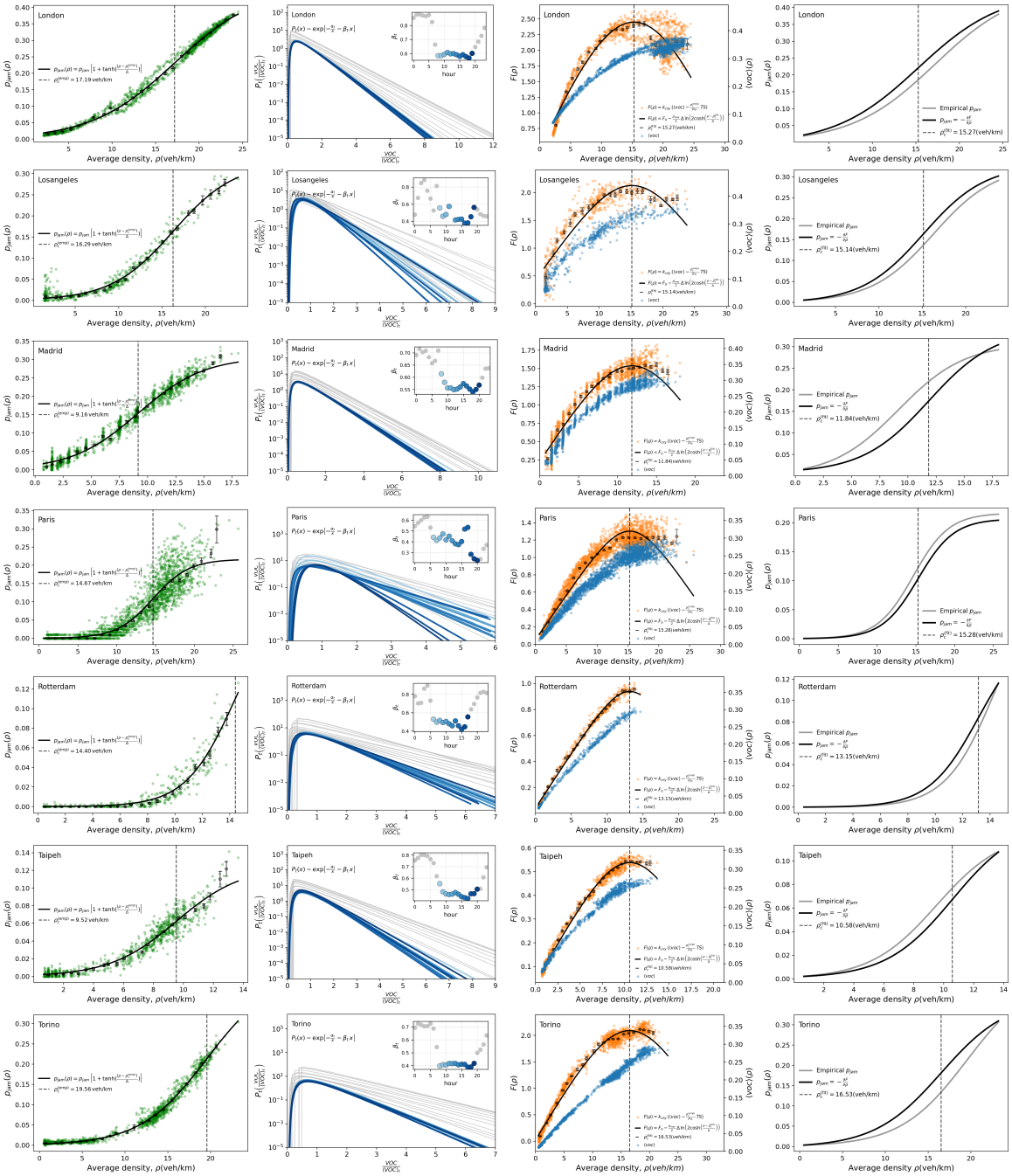

Supplementary Figure 7. Empirical reconstruction of the thermodynamic congestion framework (full panel). Each row corresponds to a city. **Left column:** Fraction of jammed links p_{jam} as a function of average network density. Points correspond to aggregated observations; solid curves show the sigmoidal fits used to extract the critical density $\rho_c^{(emp)}$. Vertical dashed lines indicate the inferred transition density. **Second column:** Hourly distributions of normalized volume-over-capacity, $x = \frac{VOC}{\langle VOC \rangle_t}$. Curves are fitted using the functional form $P_t(\mathrm{x}) \propto exp\,[-\alpha_t/x - \beta_t x]$. The inset shows the hourly variation of the decay parameter β_t, which remains approximately stable throughout the day, supporting the interpretation of $T_{VOC,t} = \frac{1}{\beta_t}$ as an effective temperature-like parameter. **Third column:** Reconstructed Helmholtz free energy $F(\rho) \sim \kappa_{city}\left(\langle VOC \rangle - \frac{\rho_c^{(emp)}}{\rho_{th}} TS\right)$ (orange, left axis) as a function of density. The black curve shows the fit $F(\rho) =$

$F_0 - \frac{p_{max}}{2}\Delta \ln\left[2cosh\left(\frac{\rho-\rho_c^{(fit)}}{\Delta}\right)\right]$. Blue points (right axis) display the average $\langle VOC \rangle$ versus density, analogous to a macroscopic fundamental diagram. In most cities, the entropic (Helmholtz) transition occurs at lower density than the peak of $\langle VOC \rangle$, indicating that configurational reorganization emerges before throughput collapse. **Right column:** Sigmoidal congestion curve reconstructed as -∂F/∂ρ, compared with the empirical p_{jam}. The agreement confirms that the observed macroscopic transition is consistent with a free-energy description.

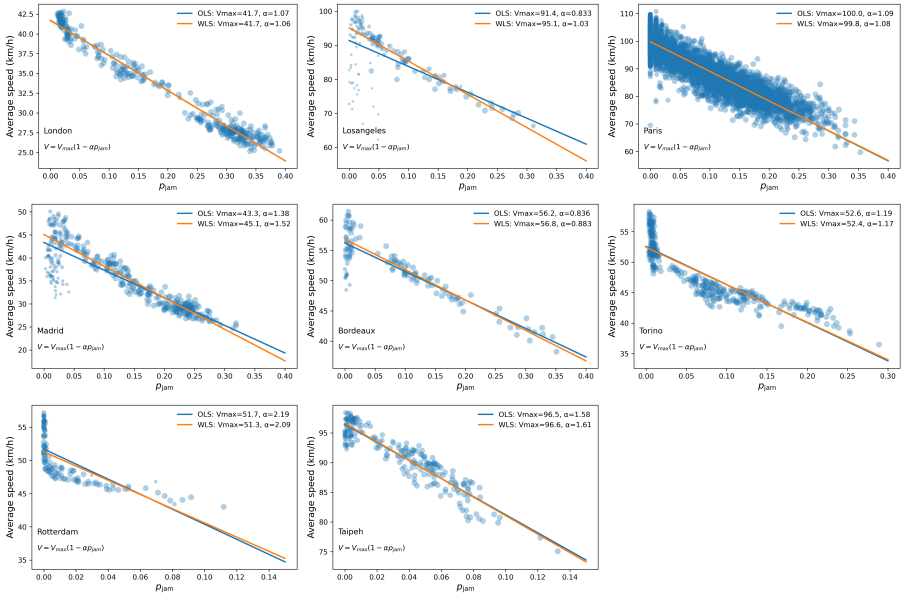

Supplementary Figure 8: Scatter plots show the relationship between the average network speed v and the fraction of congested links p_{jam} across several cities. Each point corresponds to an aggregated time interval. A clear approximately linear decrease of speed with increasing congestion is observed. The empirical relationship can be described by $v(\rho, p_{jam}) = v_{max}[1 - \gamma p_{jam}]$ where v_{max} represents the free-flow network speed and γ captures the sensitivity of the average speed to the fraction of congested links. This equation resembles the two-fluid formulation of urban traffic introduced by Prigogine and Herman (10), in which the macroscopic speed decreases proportionally to the fraction of vehicles belonging to the congested phase. Ordinary least-squares (OLS) and weighted least-squares (WLS) fits are shown for comparison across cities.

Supplementary Tables

City	Country	$p_{\max}^{(emp)}$	$\rho_c^{(emp)}$	Δ	T_{jam}	κ_{city}	$p_{\max}^{(fit)}$	$\rho_c^{(fit)}$	F_0	β	Std(β)	α	Std(α)
Paris	France	0.11	14.67	4.63	0.32	6.0	0.10	15.28	1.63	0.40	0.10	1.36	0.76
Los Angeles	US	0.16	16.29	7.12	0.44	8.0	0.16	15.14	2.94	0.47	0.07	0.87	0.28
Bordeaux	France	0.19	15.20	6.61	0.43	12.0	0.19	15.57	3.07	0.38	0.02	1.32	0.10
Taipei	Taiwan	0.06	9.52	4.42	0.46	2.4	0.07	10.58	0.74	0.46	0.02	0.86	0.09
Madrid	Spain	0.15	9.16	5.89	0.64	8.0	0.17	11.84	2.22	0.56	0.01	0.53	0.03
Rotterdam	Netherlands	0.11	14.40	3.60	0.25	3.6	0.08	13.15	1.15	0.49	0.04	0.77	0.14
London	UK	0.23	17.19	9.58	0.56	13.0	0.23	15.27	3.95	0.59	0.02	0.44	0.05
Torino	Italy	0.21	19.56	7.79	0.40	13.0	0.18	16.53	3.08	0.41	0.01	1.12	0.06

Supplemementary Table 1. Summary of fitted parameters across cities.

References

1. EL-BID/IDB-IDB-Invest-Coronavirus-Impact-Dashboard [Jupyter Notebook] [Internet]. Banco Interamericano de Desarrollo; 2026 [citado 20 de febrero de 2026]. Disponible en: https://github.com/EL-BID/IDB-IDB-Invest-Coronavirus-Impact-Dashboard

2. TomTom Traffic Index [Internet]. [citado 20 de febrero de 2026]. Traffic Index ranking. Disponible en: https://traffic-hhmw.az-weu.external.kaap.tt4.nl/traffic-index/ranking/

3. ActiveConclusion. ActiveConclusion/COVID19_mobility [Jupyter Notebook] [Internet]. 2026 [citado 20 de febrero de 2026]. Disponible en: https://github.com/ActiveConclusion/COVID19_mobility

4. COVID-19 Community Mobility Report [Internet]. [citado 24 de febrero de 2026]. COVID-19 Community Mobility Report. Disponible en: https://www.google.com/covid19/mobility?hl=en

5. Institut für Verkehrsplanung und Transportsysteme [Internet]. [citado 22 de febrero de 2026]. Makroskopische Fundamentaldiagramme. Disponible en: https://www.ivt.ethz.ch/forschung/mfd.html

6. Ambühl L, Loder A, Bliemer MCJ, Menendez M, Axhausen KW. A functional form with a physical meaning for the macroscopic fundamental diagram. Transp Res Part B Methodol. 1 de julio de 2020;Advances in Network Macroscopic Fundamental Diagram (NMFD) Research137:119-32. doi:10.1016/j.trb.2018.10.013

7. Loder A, Ambühl L, Menendez M, Axhausen KW. Understanding traffic capacity of urban networks. Sci Rep. 8 de noviembre de 2019;9(1):16283. doi:10.1038/s41598-019-51539-5

8. Ambühl L, Loder A, Menendez M, Axhausen KW. Empirical Macroscopic Fundamental Diagrams: New insights from loop detector and floating car data [Application/pdf]. enero de 2017;21 p. doi:10.3929/ETHZ-B-000167171

9. Ambühl L, Loder A, Zheng N, Axhausen KW, Menendez M. Approximative Network Partitioning for MFDs from Stationary Sensor Data. Transp Res Rec J Transp Res Board. junio de 2019;2673(6):94-103. doi:10.1177/0361198119843264

10. Herman R, Prigogine I. A Two-Fluid Approach to Town Traffic. Science. 13 de abril de 1979;204(4389):148-51. doi:10.1126/science.204.4389.148